Bound state structure and electromagnetic form factor beyond the ladder approximation

V. Gigante[a], J. H. Alvarenga Nogueira[b], E. Ydrefors[b],
C. Gutierrez[c], V.A. Karmanov[d] and T. Frederico[b] [1]

[a]*Laboratório de Física Teórica e Computacional - LFTC, Universidade Cruzeiro do Sul, 01506-000 São Paulo, Brazil*

[b]*Instituto Tecnológico de Aeronáutica, DCTA, 12228-900, São José dos Campos, Brazil*

[c]*Instituto de Física Teórica, UNESP, 01156-970, São Paulo, Brazil*

[d]*Lebedev Physical Institute, Leninsky Prospekt 53, 119991 Moskow, Russia*

Abstract

We investigate the response of the bound state structure of a two-boson system, within a Yukawa model with a scalar boson exchange, to the inclusion of the cross-ladder contribution to the ladder kernel of the Bethe-Salpeter equation. The equation is solved by means of the Nakanishi integral representation and light-front projection. The valence light-front wave function and the elastic electromagnetic form factor beyond the impulse approximation, with the inclusion of the two-body current, generated by the cross-ladder kernel, are computed. The valence wave function and electromagnetic form factor, considering both ladder and ladder plus cross-ladder kernels, are studied in detail. Their asymptotic forms are found to be quite independent of the inclusion of the cross-ladder kernel, for a given binding energy. The asymptotic decrease of form factor agrees with the counting rules. This analysis can be generalized to fermionic systems, with a wide application in the study of the meson structure.

Key words: Relativistic bound states, Bethe-Salpeter equation, Minkowski space, light-front wave function, electromagnetic form factor

The investigation of fundamental interactions faces the challenge to obtain theoretically the properties of relativistic bound systems in the Minkowski space. One relevant present example, is the introduction of quasi-parton distributions calculated with moving hadrons in the Euclidean Lattice QCD for large longitudinal momentum to match with parton distribution functions (PDFs)

[1] Corresponding author: tobias@ita.br

arXiv:1611.03773v1 [hep-ph] 11 Nov 2016

in the infinite momentum frame [1]. On the other side, recent tools are being introduced to investigate the spectrum and the Minkowski space structure of composite systems within the continuum approach to bound states in field theory, without resorting to the Wick rotation in the Bethe-Salpeter (BS) equation. One technique to solve bound and scattering problems within the BS approach relies on the Nakanishi integral representation (NIR) [2]. This method was introduced about two decades ago in [3], and further developed in [4,5] where the projection onto the light-front (LF) was used as an essential step to simplify the formalism. Later on, it was further extended to scattering states [6], and computations using convenient polynomial basis expansion were provided in [7,8]. The efforts were undertaken to invert the NIR for the Euclidean BS amplitude, in order to find the Nakanishi weight function and use it to reconstruct the BS amplitude in Minkowski space [9]. Applications to bound fermionic systems were also done [10,11]. The method has been shown to be reliable to study the spectrum and the Minkowski space structure of a relativistic two-boson system in the ladder approximation [12]. Impact parameter space amplitudes (see e.g. [13]) can be derived from the LF valence wave function of the ground and excited states. Together with the asymptotic form of the LF wave function for large transverse momentum, the impact parameter space representation at large distances were studied within the ladder approximation in [12]. The Minkowski space approach has been extended beyond the ladder exchange in Ref. [5], where it was considered the cross-ladder contribution to the kernel of the BS equation for the two-boson bound state. The binding energy as a function of the coupling constant was also computed in the Euclidean space approach within the Feynman-Schwinger framework of the Yukawa model for two-boson bound states [14], where all possible cross-ladder diagrams were taken into account. This work shows quite clearly the extra attraction provided by adding the infinite set of diagrams in the kernel of the corresponding BS equation. Indeed, the consideration of only lowest order cross-ladder diagram gives a considerable net attraction in the two-boson bound state (see e.g. [5]). Therefore, it is natural to expect that the dynamics beyond the ladder exchange is reflected not only on the binding energy but also on the Minkowski space structure of the bound state. This is modified by the higher order contributions to the kernel of the BS equation, even if the binding energy is kept fixed by changing the coupling constant.

The interesting question comes on how the dynamics beyond the ladder exchange contributes quantitatively to the asymptotic behavior of both valence LF wave function, associated with the PDFs, and to the elastic electromagnetic (EM) structure. In this paper we study the two-boson bound state structure in the Yukawa model, considering the ladder and ladder plus cross-ladder kernels, to investigate quantitatively the LF wave function and elastic EM form factor. To satisfy the gauge invariance, the cross-ladder graph must also contribute to the EM current of the bound pair as a two-body current, which is also considered in this work. These observables are intrinsically connected

with the Minkowski space structure of the bound state. The solution of the homogeneous two-boson BS equation in Minkowski space is found numerically by transforming it into a non-singular integral equation for the weight function provided by the NIR of the BS amplitude, using the technique proposed in [4,5] and further developed in [7].

To put our work on a broad perspective, we recall that in the realm of the quark counting rules [15,16] within perturbative QCD, it was derived the leading asymptotic large momentum form of amplitudes for exclusive processes, in particular to elastic form factors [17,18]. Higher-twist contributions to the associated amplitudes are subleading [17]. These ideas applied to a spin 1 two-fermion bound state resulted in the "universal ratios" [19] between the leading asymptotic contributions to the elastic EM form factors. Later on, subleading power corrections were considered in the EM form factors of the deuteron [20,21] and ρ-meson [22], and in exclusive processes [23] consistent with the LF angular conditions. Furthermore, the quark counting rules were generalized in Ref. [24] for the leading hard transverse momentum dependence of the Fock components of the hadronic LF wave function in terms of the parton number, orbital angular momentum along the z-direction and hadron helicity. The present study is a preparation for future applications to explore the nonperturbative physics of QCD. We address the issue on how the asymptotic behavior from counting rules is formed qualitatively and quantitatively, considering the NIR of the BS amplitude, both in the valence LF wave function and EM form factor. In addition, we study quantitatively the elastic two-body current associated with a cross-ladder term being a higher-twist contribution to the form factor. Our aim is to determine how it is damped with respect to the leading term in the present nonperturbative calculation of the bound state. Another aspect analyzed here is the question on how the asymptotic behavior of the form factor and LF wave function change with the modified kernel. For this study we consider a fixed binding energy, which keeps the low momentum behavior of these quantities quite independent of the kernel choice, allowing us to focus on the high momentum region independent on the binding energy.

This work is organized as follows. In Sect. 1, the BS equation and NIR of the BS amplitude are briefly introduced. In Sect. 2 the valence LF wave function is studied in detail with respect to its asymptotic form and the role of the ladder exchange in forming the leading large momentum behavior. In Sect. 3 the space-like EM form factor is introduced and the current conservation is discussed. The numerical results for the impulse and two-body current contributions to the form factor are presented, and a discussion of the ladder exchange dominance is performed quantitatively. The asymptotic behavior of the form factor is derived in Sect. 4, and we illustrate them numerically. In Sect. 5, we provide the summary and an outlook for future developments of our work.

1 Bethe-Salpeter Equation and Nakanishi Integral Representation

The BS equation in Minkowski space, for two spinless particles, reads:

$$\Phi(k,p) = S\left(\frac{p}{2}+k\right) S\left(\frac{p}{2}-k\right) \int \frac{d^4k'}{(2\pi)^4} iK(k,k',p)\Phi(k',p), \qquad (1)$$

where the Feynman propagator is $S(k) = i\left[k^2 - m^2 + i\epsilon\right]^{-1}$. The interaction kernel K is given by the sum of irreducible Feynman diagrams. The ladder kernel is considered in most of the works, but here we incorporate also the cross-ladder contribution.

The BS amplitude is found in the form of the NIR [2,3]:

$$\Phi(k,p) = -i \int_{-1}^{1} dz \int_{0}^{\infty} d\gamma \frac{g(\gamma,z)}{D^3(\gamma,z;k,p)}, \qquad (2)$$

where the Nakanishi denominator is:

$$D(\gamma,z;k,p) = \gamma + m^2 - \frac{1}{4}M^2 - k^2 - p\cdot k\ z - i\epsilon. \qquad (3)$$

The weight function $g(\gamma,z)$ itself is not singular, whereas the singularities of the BS amplitude are fully reproduced by this integral. The BS amplitude in the form (2) is substituted into the BS equation (1) and after some mathematical transformations [4], one obtains the following integral equation for $g(\gamma,z)$:

$$\int_{0}^{\infty} \frac{g(\gamma',z)d\gamma'}{\left[\gamma' + \gamma + z^2m^2 + (1-z^2)\kappa^2\right]^2} = \int_{0}^{\infty} d\gamma' \int_{-1}^{1} dz'\ V(\gamma,z,\gamma',z')g(\gamma',z'), \quad (4)$$

where for bound states $\kappa^2 = m^2 - \frac{1}{4}M^2 > 0$ and V is expressed via the kernel K. The ladder and ladder plus cross-ladder kernels in Eq. (4) were worked out in detail in Refs. [4] and [5], respectively. The numerical method to solve Eq. (4) was described in detail in [7,12], where it was proposed a basis expansion in Laguerre polynomials for the noncompact variable and Gegenbauer polynomials for the compact one.

Noteworthy to point out that the $s-$wave valence LF wave function is written in the form (we follow the convention of our previous paper [9]):

$$\psi_{LF}(\gamma,\xi) = \frac{1-z^2}{4} \int_{0}^{\infty} \frac{g(\gamma',z)d\gamma'}{\left[\gamma' + \gamma + z^2m^2 + (1-z^2)\kappa^2\right]^2}, \qquad (5)$$

where the transverse momentum is $k_\perp = \sqrt{\gamma}$ and the LF momentum fraction is $\xi = (1-z)/2$ with $0 < \xi < 1$. The physical or normal solutions of the

BS equation are the ones for which the weight function has the symmetry property $g(\gamma, z) = g(\gamma, -z)$, and it is reflected in the expected symmetry of the valence wave function for two identical bosons.

B/m	μ/m	$\alpha^{(L+CL)}$	$\alpha^{(L)}$	$\alpha^{(L)}/\alpha^{(L+CL)}$	$\psi_{LF}^{(L)}/\psi_{LF}^{(L+CL)}$
1.5	0.15	4.1399	6.2812	1.5172	1.5774
	0.50	5.1568	7.7294	1.4988	1.5395
1.0	0.15	3.5515	5.3136	1.4961	1.5508
	0.50	4.5453	6.7116	1.4766	1.5094
0.5	0.15	2.5010	3.6106	1.4436	1.4805
	0.50	3.4436	4.9007	1.4231	1.4405
0.1	0.15	1.1052	1.4365	1.2997	1.2763
	0.50	1.9280	2.4980	1.2956	1.2694

Table 1

Comparison between the ratio of the coupling constants, given in terms of $\alpha = g^2/(16\pi m^2)$, corresponding to ladder (L) and ladder plus cross-ladder (L+CL) kernels, with the ratio of the LF wave functions in the asymptotic limit, namely for a large value of $\gamma = 500m^2$, and with the particular choice $\xi = 1/2$. For this analysis we use the normalization $\psi_{LF}^{(L)}(0, 1/2) = \psi_{LF}^{(L+CL)}(0, 1/2) = 1$.

2   Valence light-front wave function

The cross-ladder kernel is attractive as it is known [5], and therefore the coupling constant decreases to keep the same binding energy, as illustrated by the values of $\alpha^{(L)}$ and $\alpha^{(L+CL)}$ presented in Table 1 for a given B and μ. The momentum dependence of the valence wave function is discussed in what follows. We choose a strongly bound situation with $B = 1.5\,m$ to show the effect of changing the interaction kernel from ladder to ladder plus cross-ladder at a fixed binding energy.

The result for the wave function is shown in Fig. 1. At relatively low momentum, $\sqrt{\gamma} \lesssim 3\,m$, the wave function is practically the same for the ladder and ladder plus cross-ladder kernels. That happens because this momentum region is determined by the binding energy that gives the behavior of the wave function at large distances. In the present case one should expect that the momentum region determined mainly by the binding energy is of the order of $\sqrt{\gamma} \sim B = 1.5\,m$, which seems to be the case. At large momentum, we observe that the ladder and ladder plus cross-ladder results for the wave function, are essentially proportional. According to the general discussion on asymptotic behavior of the LF wave function [17], the large momentum tail should be
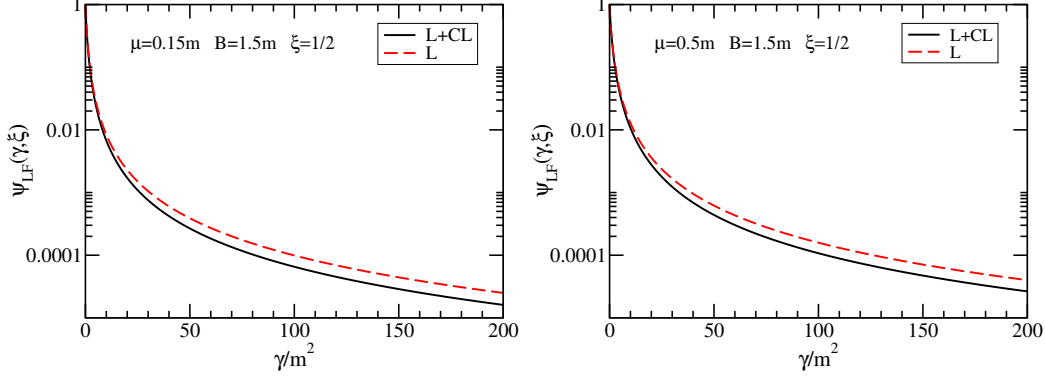
Fig. 1. LF wave function vs. γ for $\xi = 1/2$ with ladder (L) (dashed lines) and ladder plus cross-ladder (L+CL) (solid lines) interaction kernels for $B = 1.5\, m$ and $\mu = 0.15\, m$ (left-frame) and $\mu = 0.5\, m$ (right-frame).

dominated by the ladder exchange, that is common to both calculations. In [12], it was found, for ground and excited states, that for $\gamma \to \infty$:

$$\psi_{LF}(\gamma, \xi) \to \alpha\, \gamma^{-2}\, C(\xi), \tag{6}$$

where α is factorized and $\psi_{LF}(0, 1/2) = 1$ is chosen to get $C(\xi)$ in Fig. 2.

The only fact that the kernel can be enlarged to include the cross-ladder, allows us to check how $C(\xi)$ changes for a given binding energy, considering that the coupling constant has to be modified for the two kernels to keep B fixed and the ladder exchange dominates the large momentum region. Table 1 illustrates how the asymptotic wave function scales with α for ladder and ladder plus cross-ladder kernels with $\mu = 0.15\, m$ and $0.5\, m$. We considered the coupling constants for different binding energies, and the ratio of the wave functions $(\psi_{LF}^{(L)}/\psi_{LF}^{(L+CL)})$ when $\gamma = 500\, m^2$ and $\xi = 1/2$ ($z = 0$). The Table also illustrates that the ratio between the values of α are about the same as the ratio of the wave functions, namely $\alpha^{(L)}/\alpha^{(L+CL)} \approx \psi_{LF}^{(L)}/\psi_{LF}^{(L+CL)}$. This turns clear the motivation in factorizing α in Eq. (6).

The asymptotic form in Eq. (6) is also found in the Wick-Cutkosky (WC) model, where the valence ground state wave function is [25]:

$$\psi_{LF}^{(WC)}(\gamma, \xi) = \frac{C^{(WC)}(\xi)}{2\sqrt{\pi}(\gamma + m^2 - \xi(1 - \xi)M^2)^2} \tag{7}$$

with $C^{(WC)}(\xi) = \xi(1 - \xi)g^{(WC)}(1 - 2\xi)$. In the two extreme limits of binding energy, strongly and weakly bound state, this function is found analytically and it is given by

$$C^{(WC)}(\xi) = [\xi(1 - \xi)]^2, \tag{8}$$

for $B = 2\, m$, and by,

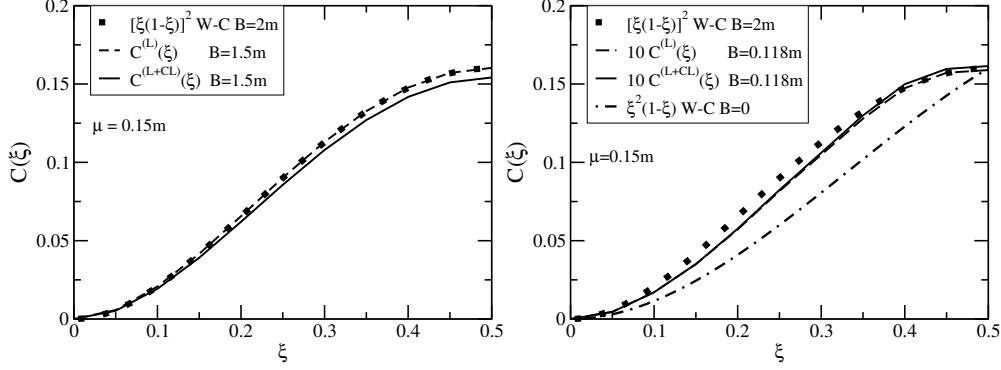$$C^{(WC)}(\xi) = \xi(1 - \xi)\left(\frac{1}{2} - \left|\frac{1}{2} - \xi\right|\right) \tag{9}$$

6

Fig. 2. Asymptotic function $C(\xi)$ defined from the LF wave function for $\gamma \to \infty$ (6) computed for the ladder kernel, $C^{(L)}(\xi)$ (dashed line), and ladder plus cross-ladder kernel, $C^{(L+CL)}(\xi)$ (solid line), with exchanged boson mass of $\mu = 0.15\,m$. Calculations are performed for $B = 1.5\,m$ (left frame) and $B = 0.118\,m$ (right frame). A comparison with the analytical forms of $C(\xi)$ valid for the Wick-Cutkosky model for $B = 2m$ (full box) and $B \to 0$ (dash-dotted line) both arbitrarily normalized.

for $B \to 0$. The normalization of $C^{(WC)}(\xi)$ presented above is chosen arbitrarily.

The asymptotic functions $C(\xi)$ defined from the LF wave function for $\gamma \to \infty$ (6) obtained with the ladder and ladder plus cross-ladder kernels are shown in Fig. 2, for weak and strong binding energies $B = 0.118\,m$ and $B = 1.5\,m$, respectively. We choose the case of an exchanged boson mass of $\mu = 0.15\,m$. As mentioned, for this study the normalization of the wave function is chosen as $\psi_{LF}(0, 1/2) = 1$. First we observe, a quite weak sensitivity in the form of $C(\xi)$ with B, for the values we use, while the Wick-Cutkosky model in the extreme limits of binding energy has $C(\xi)$ quite different as given by Eqs. (8) and (9). The noticeable difference in the weak and strong binding cases is the magnitude of $C(\xi)$, which from $B = 1.5\,m$ to $0.118\,m$ decreases by a factor of 10, considering that the normalization $\psi_{LF}(0, 1/2) = 1$ is fixed in both cases. This is the expected behavior as the wave function in the strong binding case spreads out for larger momentum than in the weak binding situation. Our results are closer to the analytical form of $C(\xi)$ obtained in the Wick-Cutkosky model for $B = 2m$. This comparison suggests that $C(\xi)$ is well approximated by $[\xi(1 - \xi)]^\lambda$ with λ close to 2 for small μ. In the extreme case of $\mu = \infty$ the asymptotic form of the LF wave function changes to γ^{-1}, while $c(\xi) = [\xi(1 - \xi)]^2$.

We remind that the end-point behavior of the LF wave function is immediately associated by Eq. (5) with the behavior of the Nakanishi weight function $g(\gamma, z)$ at $z \to \pm 1$. The quadratic form at the end point of $C(\xi)$ comes from a linear damping of $g(\gamma, z) \sim (1 - |z|)$ for $|z| \to 1$. This property will be later on used to study analytically the asymptotic form of the EM form factor and show the consistence of the formulation with the counting rules.

Our study of the structure of the bound state continues now with the analysis of the elastic EM form factor. We check the effect of the addition of the cross-ladder to the kernel, by comparing results with a fixed binding energy. We explore the low and high momentum transfer regions, with the aim to verify the asymptotic behavior and the dominance of the ladder exchange for large momentum. Furthermore, the ladder plus cross-ladder kernel offers the opportunity to study the effect of the two-body current in the form factor and we show analytically and quantitatively its faster decay with momentum transfer, as it is expected from a higher-twist contribution to the form factor [17].

3   Space-like Electromagnetic Form factor

For a spinless system in the general case the e.m. current (not necessary elastic and conserved) is given by

$$J_\mu = (p_\mu + p'_\mu)F_1(Q^2) + (p_\mu - p'_\mu)F_2(Q^2)\,, \tag{10}$$

where $Q^2 = -(p - p')^2 > 0$. In the elastic case current conservation implies that $F_2 = 0$ and only F_1 survives and represents the virtual photon absorption amplitude by the composite system.

For our kernel considered up to the cross-ladder the gauge invariance of the EM coupling implies two irreducible contributions to the photon absorption amplitude, which leads to two parts of the form factors

$$F_1(Q^2) = F_I(Q^2) + F_X(Q^2), \tag{11}$$

where F_I means the impulse contribution, obtained from the triangle diagram, Fig. 3 (left), and F_X is the two-body current contribution to the form factor, which is computed from the virtual photon absorption amplitude diagrammatically depicted in Fig. 3 (right).
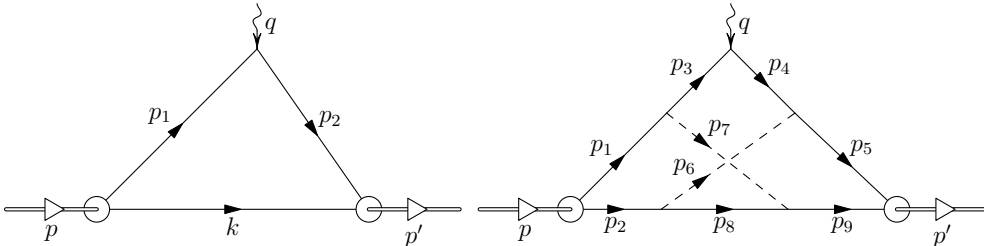

Fig. 3. Diagrammatic representation of the photon absorption amplitude: impulse (left) and two-body current contribution (right).

3.1 Impulse contribution to the form factor

The impulse contribution to the form factor is represented diagrammatically in Fig. 3. For a system composed of two spinless particles, the EM vertex can be expressed in terms of the BS amplitude by the formula

$$(p+p')^\mu F_I(Q^2) = i \int \frac{d^4k}{(2\pi)^4}(p+p'-2k)^\mu \, (k^2-m^2) \, \Phi\left(\frac{p}{2}-k,p\right) \Phi\left(\frac{p'}{2}-k,p'\right). \tag{12}$$

We contract both sides of (12) with $(p+p')_\mu$ and substitute in its r.h.-sides the BS amplitude in terms of the NIR given in Eq. (2):

$$F_I(Q^2) = \frac{i}{(2\pi)^4} \int_0^\infty d\gamma \int_{-1}^1 dz \int_0^\infty d\gamma' \int_{-1}^1 dz' \int d^4k \left[1 - \frac{2k\cdot(p+p')}{(p+p')^2}\right]$$
$$\times \frac{(m^2-k^2)\,g(\gamma,z)g(\gamma',z')}{D^3(\gamma,z;\frac{p}{2}-k,p)\,D^3(\gamma',z';\frac{p'}{2}-k,p')}, \tag{13}$$

D is defined in (3). The loop integral in d^4k is calculated analytically by means of the Feynman parametrization. This procedure is described in detail in Ref. [26]. In this way, one finds the exact formula in terms of the weight function $g(\gamma,z)$:

$$F_I(Q^2) =$$
$$= \frac{1}{2^7\pi^3} \int_0^\infty d\gamma \int_{-1}^1 dz\, g(\gamma,z) \int_0^\infty d\gamma' \int_{-1}^1 dz'\, g(\gamma',z') \int_0^1 dy\, y^2(1-y)^2 \frac{f_{num}}{f_{den}^4}, \tag{14}$$

where

$$f_{num} = (6\eta-5)m^2 + [\gamma'(1-y)+\gamma y](3\eta-2) + 2M^2\eta(1-\eta)+$$
$$+ \frac{1}{4}Q^2(1-y)y(1+z)(1+z')$$
$$f_{den} = m^2 + \gamma'(1-y) + \gamma y - M^2(1-\eta)\eta + \frac{1}{4}Q^2(1-y)y(1+z)(1+z'), \tag{15}$$

with $2\eta = (1+z)y + (1+z')(1-y)$.

3.2 Two-body current contribution to the form factor

Next, we sketch the computation of the form factor for the two-body current represented by the diagram shown in the right of Fig. 3, where the photon vertex is given by $-i(p_4+p_3)^\mu$. The form of the two-body current in terms of

the BS amplitudes of the final and initial state is written as:

$$F_X(Q^2) = -i\frac{g^4}{(2\pi)^{12}} \int d^4p_2 d^4p_8 d^4p_9 \left[1 - 2\frac{(p+p')\cdot(p_9+p_2-p_8)}{(p+p')^2} \right]$$

$$\times \left[\prod_{i=3,i\neq 5}^{8} \frac{1}{p_i^2 - m_i^2 + i\epsilon} \right] \Phi\left(\frac{p}{2} - p_2, p\right) \Phi\left(\frac{p'}{2} - p_9, p'\right) , \quad (16)$$

where $p_3 = p - p_9 - p_2 + p_8$, $p_4 = p' - p_9 - p_2 + p_8$, $p_6 = p_2 - p_8$, $p_7 = p_9 - p_8$, $m_3 = m_4 = m$ and $m_6 = m_7 = \mu$.

After substituting the BS amplitude by the NIR, Eq. (2), in the above formula, and using six Feynman parametric integrations, only one denominator remains, and by standard integrations over the three loops one obtains

$$F_X(Q^2) = -\frac{3\alpha^2 m^4}{(2\pi)^5} \int_0^\infty d\gamma \int_{-1}^1 dz \int_0^\infty d\gamma' \int_{-1}^1 dz' g(z',\gamma')g(z,\gamma)$$

$$\times \prod_{i=1}^6 \int_0^1 dy_i \Theta\left(1 - \sum_{j=i+1;i<4}^4 y_j\right) (1-y_5)^2 y_5^2 (1-y_6)^2 y_6^3 \frac{f_{num}^X}{[f_{den}^X]^5}, \quad (17)$$

where the functions f_{num}^X and f_{den}^X, depends on the m, y_i, γ, z, γ', z', p' and p. They do not contain any singularity, but are too lengthy to be explicitly shown here. For the calculation of the form factor the above formula is used.

Current conservation. The expression for the elastic EM vertex is symmetric relative to the permutation $p \leftrightarrow p'$ both for the impulse as well as for the two-body current contributions. Hence, the second (antisymmetric) term in (10) cannot appear in the elastic EM vertex, and therefore $F_2(Q^2) \equiv 0$. That follows from the contraction of the EM vertices associated with the impulse and two-body current terms, diagrammatically shown in Fig. 3, with $(p-p')^\mu$, which results in zero for any BS amplitude in the elastic case. In this case current conservation is automatically fulfilled for any particular contribution to the current.

However, J_μ is an operator and the current conservation $J \cdot q = 0$ means that all the matrix elements of this operator must be zero. What we considered for elastic form factor is only one (diagonal) matrix element. The non-diagonal (transition) matrix elements bound $\rightarrow$ excited state also must be zero. The above symmetry will not hold in this case and the zero value of $J \cdot q$ should appear as a subtle cancellation of different contributions both in the kernel and in the EM vertex. This cancellation found numerically would be indeed a powerful test, as in Ref. [27], where this cancellation was demonstrated numerically for the transition form factor associated with the EM breakup process: bound $\rightarrow$ scattering state. In the present work we restrict ourselves by the elastic case only. The inelastic transitions and the current conservation in this case will be a subject of forthcoming paper.
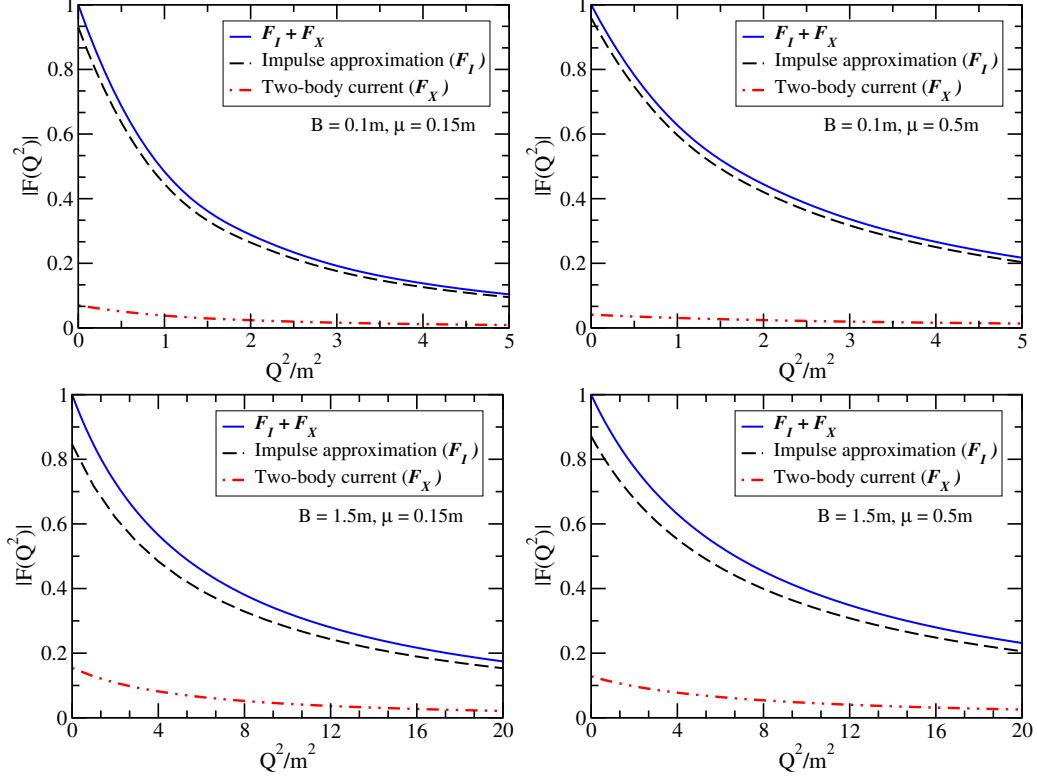
Fig. 4. Form factor as a function of Q^2. Calculations performed with the BS amplitude from the ladder plus cross-ladder kernel. The solid curve is the full form factor. The dashed curve is the impulse contribution (F_I). The double-dotted dashed curve is the two-body current (F_X) contribution to the EM vertex. Results for: $B = 0.1\,m$ and $\mu = 0.15\,m$ (upper-left frame), $B = 0.1\,m$ and $\mu = 0.5\,m$ (upper-right frame), $B = 1.5\,m$ and $\mu = 0.15\,m$ (lower-left frame), $B = 1.5\,m$ and $\mu = 0.5\,m$ (lower-right frame).

3.3 Results for the impulse and two-body current form factors

In Fig. 4, we present the impulse (F_I) and two-body current contributions (F_X) to the form factor, diagrammatically depicted in Fig. 3, and computed with Eqs. (14) and (17), respectively. The calculations are performed for two representative binding energies $B = 0.1\,m$ and $1.5\,m$, namely weak and strong binding cases, respectively. For both cases, the calculations are carried out with the BS amplitude obtained with the ladder plus cross-ladder kernel in Eq. (4) for exchanged boson mass of $\mu = 0.15\,m$ and $\mu = 0.5\,m$. The solid curve everywhere is the total form factor, normalized to one at $Q^2 = 0$. The total form factor is the sum of F_I (dashed curve) and the F_X (double dot-dashed curve) contributions to the EM vertex. We see that the relative contribution of F_X increases when μ decreases for a given B, as the overlap between the two-body current operator and the BS amplitude increases, once the size of the state is fixed essentially by B. The same reason explains that by increasing the

binding energy the magnitude of the contribution of the two-body current to the form factor increases. Indeed, in the case that we presented the maximal contribution is at $Q^2 = 0$ of F_X (about 15% from the total form factor) achieved for $\mu = 0.15\,m$ and $B = 1.5\,m$. This indicates that the two-body current operator contributes to short distance physics, as one could expect.

Another feature one can extract by inspecting Fig. 4, is the role of the ladder exchange in shaping the large momentum region of F_I for $Q^2 > \mu^2$, m^2 (later on we will discuss in more details the asymptotics of the form factors). For a given binding energy, the change of μ modifies considerably the form factor, which essentially is dominated by the impulse contribution for the large momentum region, as for instance, in the case of $B = 0.1\,m$, presented in the upper frames of Fig. 4. In addition, the dominance of the ladder exchange in forming the tail of the form factor is evident, and for $Q^2/m^2 = 20$ one sees a scaling with α, which changes by about a factor of about two when μ goes from $0.15\,m$ to $0.5\,m$ (see Table 1). This feature at large momentum is independent on the binding energy, as is exemplified, in the lower frames of Fig. 4 for $B = 1.5\,m$. The same property is found at large transverse momentum for the LF wave function as given by Eq. (6). It is important to point out that the binding energy is fixed, which shapes the low momentum region of the wave function, and also to some extent the form factor.

In Fig. 5 we study the sensitivity of the form factor to the dynamics, namely using the BS amplitude computed with ladder or with ladder plus cross-ladder kernels, for fixed binding energy of $B = 1.5\,m$ and exchange boson masses of $\mu = 0.15\,m$ and $0.5\,m$. We choose the momentum transfer interval of $0 \leq Q^2/m^2 \leq 50$. We start by comparing the ladder results for the form factor with the one obtained for the ladder plus cross-ladder kernel, considering the full current in both cases. We observe at low momentum, below m, very similar slopes, that reflects close charge radius and the bound state size, which is determined by the same binding energy. This finding is independent of the mass of the exchanged boson, as one can verify by inspecting the right and left panels of Fig. 5. Comparing both frames, one observes that while the slopes are similar by changing μ, the form factor at large momentum approximately scales with α, which we have already discussed together with Fig. 4, and the dominance of the ladder exchange in the structure of the state at large momentum.

We also compare the impulse contribution for the ladder and ladder plus cross-ladder kernels in Fig. 5, which are represented by the dot-dashed lines. For that purpose both are normalized to one at zero momentum transfer. We notice two interesting features: (i) the slope is the same for $Q \lesssim m$; (ii) at large momentum the inclusion once properly normalized the impulse contribution dominates. The first point (i), comes from the fact that the binding energy essentially fixes the structure at low momentum, the second point (ii), comes

from the fact that the two-body current decreases much faster than the impulse contribution, as the former is a higher-twist contribution to the photon absorption process. Indeed for large momentum the two-body current decays as Q^{-2} with respect to the impulse contribution, which will be shown in detail in what follows.
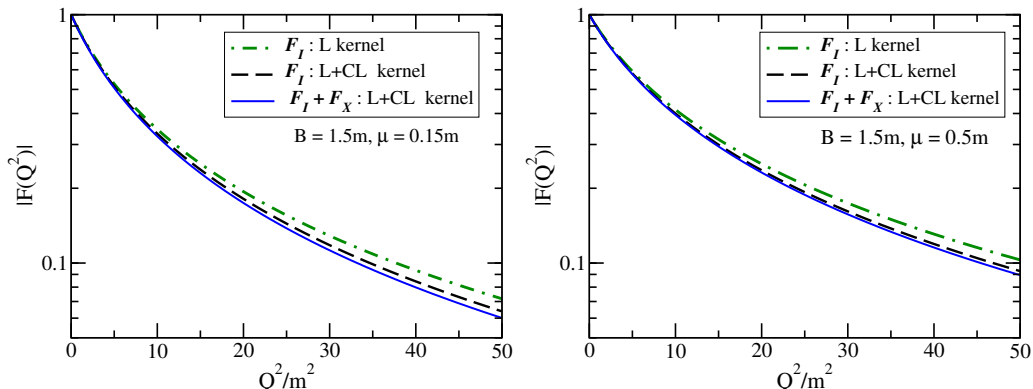

Fig. 5. Form factor as a function of Q^2. The dot-dashed curve is the form factor calculated with the BS amplitude found for ladder (L) kernel. The dashed curve is the impulse contribution to the form factor computed with the BS amplitude obtained with the ladder plus cross-ladder (L + CL) kernel. The solid curve is the full form factor obtained from the BS amplitude calculated with L + CL kernel. The binding energy is $B = 1.5\,m$, with the mass of the exchanged boson $\mu = 0.15\,m$ (left-frame) and $\mu = 0.5\,m$ (right-frame). All curves are normalized to 1 at $Q^2 = 0$.

4 Asymptotic behavior of the form factor

The leading behavior of the impulse and two-body current contributions to the form factors for $Q^2 \to \infty$ can be obtained by using standard counting rules [17]. In order to find the leading power law behavior of the form factors represented in Figs. 4 and 5, one has to count the number of propagators, in which the large virtual photon momentum flows between the emission and absorption by the constituents in the bound state. This counting is provided, of course, by our formalism and it results in

$$F_I(Q^2) \sim Q^{-4} \quad \text{and} \quad F_X(Q^2) \sim Q^{-6}, \tag{18}$$

apart from logarithmic corrections (see e.g. [25]). The two-body current is identified with a higher twist contribution and decreases faster than the impulse term by a Q^{-2} factor. To illustrate in a transparent and analytical way how such asymptotic behavior of the form factors arises, we analyze it using directly Eqs. (13) and (16) in the following.

13

4.1 $F_I(Q^2)$ at large Q^2

We work in the Breit reference frame, where $\vec{p} = -\vec{p'} \equiv \vec{n}p_v$, $p_0 = p_0' = \sqrt{M^2 + p_v^2}$, $Q^2 = -(p'-p)^2 = 4p_v^2$ and $\vec{n}$ is the direction of the incident momentum $\vec{p}$. Hence $p_v = \frac{1}{2}Q$, $p_0 = p_0' = \sqrt{M^2 + \frac{1}{4}Q^2}$ in Eq. (13). We also denote $|\vec{k}| = k_v$. Substituting these expressions into the functions $D(\gamma, z; \frac{p}{2} - k, p)$ appearing in the denominator of Eq. (13), at large Q we get:

$$D(\gamma, z; \frac{p}{2}-k, p) \approx (k_0 - \vec{n}\cdot\vec{k})(1+z)\frac{Q}{2} + \gamma - k_0^2 + k_v^2 + m^2 - i\epsilon - \frac{1}{2}M^2(1+z), \quad (19)$$

and similarly for $D(\gamma', z'; \frac{p'}{2} - k, p')$. Omitting a factor, we can represent the denominators in (13) as:

$$D(\gamma, z; \frac{p}{2} - k, p) \propto (1+z)Q + \delta, \quad D(\gamma', z'; \frac{p'}{2} - k, p') \propto (1+z')Q + \delta', \quad (20)$$

where δ, δ' do not depend on Q. Hence

$$F_I(Q^2) \propto \int_{-1}^{1} \frac{g(z)dz}{[(1+z)Q + \delta]^3} \int_{-1}^{1} \frac{g(z')dz'}{[(1+z')Q + \delta']^3} =$$
$$= \frac{1}{Q^6} \int_{-1}^{1} \frac{g(z)dz}{\left(1 + z + \frac{\delta}{Q}\right)^3} \int_{-1}^{1} \frac{g(z')dz'}{\left(1 + z' + \frac{\delta'}{Q}\right)^3}, \quad (21)$$

where the variables γ, γ' and the integration over k are omitted since they give a finite corrections making no influence on the asymptotic behavior of the form factor.

If we put $\frac{\delta}{Q} = 0$ in Eq. (21), we get a divergent integral at $z = -1$. This means that the decreasing of the factor $\frac{1}{Q^6}$ can be compensated by an increasing of the values of the integrals at finite Q^2. Indeed, for $g(z) \equiv 1$, the integral has the form:

$$\int_{-1}^{1} \frac{dz}{\left(1 + z + \frac{\delta}{Q}\right)^3} \sim \frac{Q^2}{2\delta^2}. \quad (22)$$

For $g(z) \equiv 1$ it gives the asymptotic form factor as $F_I(Q^2) \propto 1/Q^2$. However, the function $g(z)$ tends linearly to zero as $z \to -1$: $g(z) \sim (1+z)$. This weakens the compensation, therefore:

$$\int_{-1}^{1} \frac{g(z)dz}{\left(1 + z + \frac{\delta}{Q}\right)^3} = \int_{-1}^{1} \frac{(1+z)dz}{\left(1 + z + \frac{\delta}{Q}\right)^3} \sim \frac{2Q}{\delta}. \quad (23)$$

This provides the asymptotic behavior:

$$F_I(Q^2) \propto Q^{-4}. \quad (24)$$

We can summarize the origin of this result as follows: the denominator of each propagator, containing p or p', according to (20), contributes the factor $\sim Q$ (if the limit $Q \to \infty$ does not create a divergence). In (13) we have two such propagators, each in 3rd degree ($\sim \frac{1}{D^3 D'^3}$). This gives the factor $\sim \frac{\delta^6}{Q^6}$ in (21). In the case of divergence (at $Q \to \infty$), like

$$\int_{-1} \frac{dz}{(1+z)^2} = -\frac{1}{1+z}\bigg|_{z\to -1}, \tag{25}$$

large but finite value of Q eliminates the divergence, automatically replacing the limit $z = -1$ by the cutoff $z = -1 + \frac{\delta}{Q}$. The integral becomes to be finite but large: $\sim \frac{Q}{\delta}$. In (21) the product of two such integrals results in the factor $\sim \frac{Q^2}{\delta^2}$. This weakens the falloff $\sim \frac{1}{Q^6}$ up to $F(Q^2) \propto \frac{1}{Q^4}$ in (13).

Except for the term $\sim \log\left(\frac{Q^2}{m^2}\right)$ (which is out of the precision of this consideration) the asymptotic behavior $F_I(Q^2) \propto \frac{1}{Q^4}$ coincides with the form factor fall-off found in Eq. (28) of Ref. [25] for the Wick-Cutkosky model. The agreement of Eq. (24) with the asymptotic behavior found in [25] confirms the validity of the present consideration. Below we will apply this method to the two-body current contribution.

4.2 $F_X(Q^2)$ at large Q^2

The two-body current to the EM form factor is shown in Fig. 3. As independent integration variables we chose the four-momenta p_2, p_8, p_9. The other momentas are expressed as: $p_1 = p - p_2$, $p_5 = p' - p_9$, $p_6 = p_2 - p_8$, $p_7 = p_9 - p_8$, $p_3 = p - p_2 - p_9 + p_8$, $p_4 = p' - p_2 - p_9 + p_8$. The arguments of the BS amplitudes are: $k = \frac{1}{2}(p_1 - p_2) = \frac{1}{2}p - p_2$, $k' = \frac{1}{2}(p_5 - p_9) = \frac{1}{2}p' - p_9$. Then the two-body current in the form factor is given by Eq. (16). It should be noticed that the arguments of the BS amplitudes in this equation are $\frac{p}{2} - p_2$ and $\frac{p'}{2} - p_9$. At large Q^2 we omit the factors $(p' + p)^2$ and $[(p' + p)^2 - 2(p + p')\cdot(p_9 + p_2 - p_8)]$. We can also omit the propagators carrying the momenta p_6, p_7 and p_8.

The first two (cubic) factors in (16) coming from the NIR of the two BS amplitudes have the same form as the corresponding factors in (13). Applying to them the analysis performed for F_I, we find that the product of them results in $\sim \frac{1}{Q^4}$. However, Eq. (16) contains two additional propagators with p and p', associated with p_3 and p_4. They result in an asymptotic behavior similar to (20), but without the factors $(1 + z)$, $(1 + z')$. Hence, each of them adds one extra factor $\frac{1}{Q}$. They together give two extra powers of momentum $\sim \frac{1}{Q^2}$. Hence, the degree $\frac{1}{Q^4}$ is replaced by $\sim \frac{1}{Q^6}$. We conclude that the two-body current has the asymptotic behavior $F_X(Q^2) \propto Q^{-6}$, consistent with the counting rules. We stress that the asymptotic forms depend crucially on the

15

end-point behavior of the weight function, which is immediately translated to the valence wave function, as seen in Eq. (5).
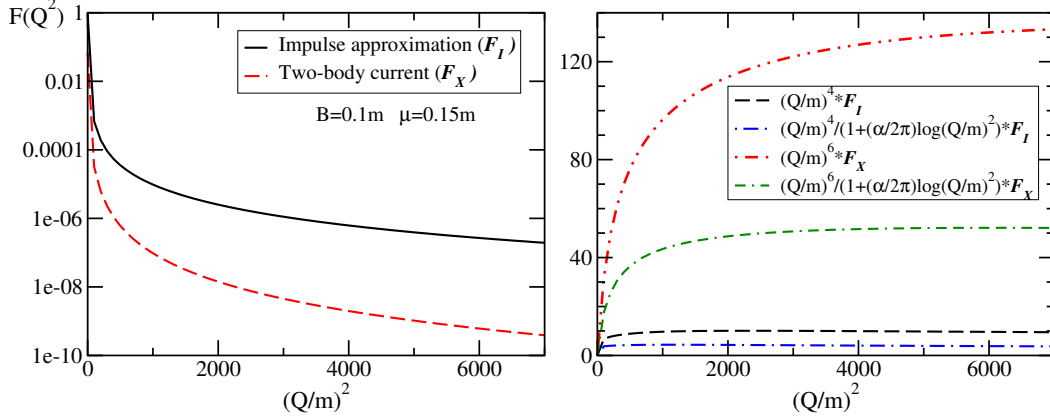

Fig. 6. EM form factor for the case $\mu = 0.15\,m$ and $B = 0.1\,m$ obtained with the ladder plus cross-ladder kernel. In the left-frame the two contributions of the form factor are displayed. In the right-frame the asymptotic behaviors of the corresponding contributions are analyzed.

4.3 Form factors at large Q: some numerical results

The asymptotic behavior of the form factors given in (18) are illustrated in Fig. 6. The calculations are done with the ladder plus cross-ladder kernels with $\mu = 0.15\,m$ and $B = 0.1\,m$. The results for F_I and F_X normalized according to Fig. 4 are shown. We perform an extensive exploration for very large momentum transfers to check as well the leading log corrections to the form factors. We have not derived these corrections for the form factor and just use it as suggested from the Wick-Cutkosky model, as derived in [25]. We perform four studies devoted to single out the asymptotic behavior of F_I and F_X: (i) $Q^4\,F_I$, (ii) $Q^6\,F_X$, (iii) $Q^4/\left[1 + (\alpha/2\pi)\log(Q/m)^2\right]\,F_I$, and (iv) $Q^6/\left[1 + (\alpha/2\pi)\log(Q/m)^2\right]\,F_X$. We first observe that the asymptotic region is established for $Q/m \sim 30$, which seems reasonable as all involved scales, masses and binding energy are of order m. Second, the products (i) and (ii) are slowly decreasing, while (iii) and (iv), with the inclusion of the leading log correction, which we can distinguish in so large momentum transfer interval presented in Fig. 6, show an improvement in getting the flat behavior at large momentum.

5 Summary and outlook

The response of the Minkowski space structure of a two-boson bound state, within a Yukawa model with a scalar boson exchange, to the inclusion of the

cross-ladder contribution to the ladder kernel of the BS equation was investigated quantitatively. The NIR allied with the LF projection was used to solve numerically the BS equation in Minkowski space. We computed both the valence wave function and elastic electromagnetic form factor including the two-body current contribution to the electromagnetic vertex. We have discussed in detail the dependence on the ladder exchange in building the asymptotic behavior of the valence wave function and form factor, for a fixed binding energy, considering both ladder and ladder plus cross-ladder kernels. This allowed us to single out the dominance of the ladder exchange, by comparing results for a fixed binding energy and using the two interacting kernels.

The valence wave function at low transverse momentum is independent of the kernel, being determined just by the given binding energy. We also studied quantitatively the factorization of the valence wave function in terms of the transverse and longitudinal momenta at large transverse momentum [12]. In this case, as expressed by Eq. (6), once α is factorized out for both binding energy and normalization fixed, the form of the wave function with the longitudinal momentum fraction is quite universal. In the case of $B/m > 0.1$, we found that the functional form approaches the Wick-Cutkosky solution $[\xi(1-\xi)]^2$ obtained for $B = 2m$ in Ref. [25]. Our conjecture is that the form and magnitude of $C(\xi)$ and the wave function at low transverse momentum, for the normalization $\psi_{LF}(0, 1/2) = 1$ and a given binding energy, are to great deal independent on the inclusion of the irreducible cross-ladder contributions in higher order in the kernel. Then, we can turn our attention to the nice work [14], where the problem with the generalized ladder kernel was solved by means of the Feymman-Schwinger representation. Making use of that, one can speculate on the form of the valence wave function when an infinite set of cross-ladder diagrams are included in the kernel.

The electromagnetic current in the case of the cross-ladder kernel includes, besides the impulse term, a two-body current obtained by gauging the cross-ladder kernel. We note that due to the symmetry of the elastic virtual photo-absorption amplitude, the impulse and two-body amplitudes, conserve current independently, which is not the case in an inelastic transition. Our numerical results show that for a given binding energy, the two-body current becomes more relevant as lighter is the exchanged boson mass as well as when the binding energy becomes larger. This is easy to understand if one considers that in both cases the overlap between the bound state and the two-body current increases, either by increasing the range of the interaction or decreasing the size of the bound state. For zero momentum transfers, where the two-body current is more relevant, and for a strongly bound system the contribution is about 15 % of the normalization.

The form factor in the large momentum region was studied in detail and the power-law decreasing, as expected from the counting rules applied to our

17

model, was derived using the adopted Nakanishi integral representation of Bethe-Salpeter amplitude. The leading contribution to the dependence on the large momentum transfer comes from the ladder exchange, which was illustrated by comparing the impulse term from ladder and ladder plus cross-ladder kernels, where the proportionality of the tail to α was singled out for a fixed binding energy. It was pointed out the crucial role of the end-point behavior of the Nakanishi weight function in the power-law behavior.

Although, the present study is focused on the two-boson problem, the present analysis can be extended to fermionic systems, for which the Bethe-Salpeter amplitude has been obtained by means of the Nakanishi representation [10,11]. It has of course wide applications to the study of meson structure.

References

[1] X. Ji, Phys. Rev. Lett. **110** (2013) 262002

[2] N. Nakanishi, Phys. Rev. **130** (1963) 1230; N. Nakanishi, Prog. Theor. Phys. Suppl. **43** (1969) 1; Graph Theory and Feynman Integrals (Gordon and Breach, New York, 1971).

[3] K. Kusaka and A. G. Williams, Phys. Rev. D **51** (1995) 7026; K. Kusaka, K. Simpson and A. G. Williams, Phys. Rev. D **56** (1997) 5071.

[4] V. A. Karmanov and J. Carbonell, Eur. Phys. J. A **27** (2006) 1.

[5] J. Carbonell, V. A. Karmanov, Eur. Phys. J. A **27** (2006) 11.

[6] T. Frederico, G. Salmè and M. Viviani, Phy. Rev. D **85** (2012) 036009.

[7] T. Frederico, G. Salmè and M. Viviani, Phy. Rev. D **89** (2014) 016010.

[8] T. Frederico, G. Salmè and M. Viviani, Eur. Phys. J. C **75** (2015) 398.

[9] T. Frederico, J. Carbonell, V. Gigante and V.A. Karmanov, Few-Body Syst. **56** (2016) 549.

[10] J. Carbonell, V.A. Karmanov, Eur. Phys. J. A **46** (2010) 387.

[11] W. de Paula, T. Frederico, G. Salmè, M. Viviani, Phys. Rev. D **94** (2016) 071901.

[12] C. Gutierrez, V. Gigante, T. Frederico, G. Salmè, M. Viviani, L. Tomio, Phys. Lett. B **759** (2016) 131.

[13] M. Burkardt, Int. J. Mod. Phys. A **18** (2003) 173.

[14] T. Nieuwenhuis and J. A. Tjon, Phys. Rev. Lett. **77** (1996) 814.

[15] B. A. Matveev, R. M. Muradjan and A. N. Tavkhelidze, Lett. Nuov. Cim. **7** (1973) 719.

[16] S. J. Brodsky and G. R. Farrar, Phys. Rev. Lett. **31** (1973) 1153.

[17] G. P. Lepage and S. J. Brodsky, Phys. Rev. D **22** (1980) 2157

[18] S. J. Brodsky, C.-R. Ji, Phys. Rev. Lett. **55** (1985) 2257.

[19] S. J. Brodsky and J. R. Hiller, Phys. Rev. D **46** (1992) 2141.

[20] A. P. Kobushkin and A. I. Syamtomov, Phys. Rev. D **49** (1994) 1637.

[21] A. P. Kobushkin and A. I. Syamtomov, Phys. Atom. Nucl. **58** (1995) 1477.

[22] J.P.B.C. de Melo, Chueng-Ryong Ji, T. Frederico, Phys. Lett. **B** 763 (2016) 87.

[23] C. E. Carlson and C.-R. Ji, Phys. Rev. D **67** (2003) 116002.

[24] X. Ji, J.-P. Ma, and F. Yuan, Phys. Rev. Lett. **90** (2003) 241601.

[25] D. S. Hwang and V.A. Karmanov, Nucl. Phys. B **696** (2004) 413.

[26] J. Carbonell, V. A. Karmanov and M. Mangin-Brinet, Eur. Phys. J. A **39** (2009) 53.

[27] J. Carbonell and V.A. Karmanov, Phys. Rev. D **91** (2015) 076010.